RESEARCH ARTICLE

Influence of the concentration of capping agent on synthesizing and analyses of Ceria nano-filler using modified co-precipitation technique

Ramachandran Murugesan[1,2] | **Subadevi RengaPillai**[1] | **Rajkumar Palanisamy**[1] |
Muthupradeepa Rajendran[1,3] | **Yuvakkumar Rathinam**[1] | **Sivakumar Marimuthu**[1] 🔘

[1]Energy Material Lab, Department of Physics, Science Block, Alagappa University, Karaikudi, India

[2]Department of Physics, Arumugam Pillai Seethai Ammal College, Tiruppattur, India

[3]Department of Physics, Science and Humanities, Sree Sastha Institute of Engineering and Technology, Chennai, India

Correspondence
Sivakumar Marimuthu, Energy Material Lab, Department of Physics, Science Block, Alagappa University, Alagappa University, Karaikudi 630 003, Tamil Nadu, India.
Email: susiva73@yahoo.co.in; sivakumarm@alagappauniversity.ac.in

Funding information
Ministry of Human Resource Development, Grant/Award Number: F-24-51/2014 U; Department of Science and Technology, Ministry of Science and Technology, Grant/Award Number: EMR/2016/006302; University Grants Commission, Grant/Award Number: F.No.41.839/2012(SR)

Abstract

The pure crystalline cerium oxide (CeO_2) nanoparticles were synthesized using optimized content of $Ce(NO_3)_3 \cdot 6H_2O$ with varying concentrations of sodium hydroxide (NaOH) (0.5, 1, 1.5, and 2 M) as a precipitation agent in presence of 2.5 wt% poly(vinylpyrrolidone) PVP. All the samples are prepared via the modified coprecipitation technique. The synthesized materials have been analyzed using X-ray diffraction (XRD), Fourier transform infrared (FT-IR), laser Raman, high-resolution scanning electron microscope (HR-SEM), and photo luminescence (PL) analyses. The optimized sample was identified with the help of the above studies that could be analyzed through transverse electron microscopy (TEM) and X-ray photoelectron spectroscopy (XPS) studies. The cubic structure with the Fm-3 m space group has been confirmed through XRD (JCPDS: 81-0792) and Raman analyses. The FT-IR and energy dispersive X-ray spectroscopy (EDX) analyses ascertain the occurrence of Ce and O species. The as-prepared CeO_2 filler (0, 3, 6, 9, and 12 wt%) is dispersed through the optimized polymer electrolyte Poly (styrene-co-methyl methacrylate) P(S-MMA) (27 wt%)–lithium perchloride ($LiClO_4$) (8 wt%)–ethylene carbonate + propylene carbonate (EC + PC) (1;1 of 65 wt%) complex system using solution casting technique. P(S-MMA) (27 wt%)–$LiClO_4$ (8 wt%)–EC + PC (1;1 of 65 wt%)–6 wt% of CeO_2 shows the high ionic conductivity 8.13×10^{-4} S cm^{-1}.

KEYWORDS
capping agent, cerium oxide, modified co-precipitation method, poly (vinyl) pyrrolidone, sodium hydroxide

1 | INTRODUCTION

The growing liveliness demands of the recent globe inspire scientists to pursuit a substitute energy foundation. Lithium batteries (LiBs) have been alleged to the substitute energy sources, owing to their greater possessions such as large energy density, huge power density for the uses in mobile phones to plug-in cars.[1] Transporting path is a significant portion of

the LiBs, and it secures to drift of ions and also restricts the internal short circuiting. The use of solid electrolytes in lithium secondary batteries provides rewards of simple cell design, airtight, extensive working array, fire-proof, and no air evolution related to organic electrolyte.[2] Blending and adding plasticizers are the accepted practices; it is simple to regulate the characteristics and improves the room temperature conductivity of ions by diminishing the degree of crystallinity

of the electrolyte matrices, although conductivity of ions and thermal and tensile constancy has been still under the lower magnitude of commercial usages. Henceforth, to increase the conductivity of ions has been synthesized by the inclusion of the nanofiller such as silicon dioxide (SiO_2), cerium oxide (CeO_2), titanium dioxide (TiO_2), zirconia (ZrO_2), and alumina (Al_2O_3) in the polymer matrix.[3,4] Among these, cerium oxide (CeO_2, Ceria) is a technologically important ceramic material, because of its high dielectric constant ($\varepsilon = 26$) and high bandgap energy.[5] It is also the most abundant rare earth element present around 66 fragments per million in the ground's crust. Cerium oxide has a fluorite-like cubic structure. Recently, cerium oxide has been used in multiple applications such as gas sensors, fuel cells, energy storage materials, and catalysis.[6] Most of the results have exposed that the wide uses of cerium oxide, because of its relative abundance, exclusive acid-base surface characters with the energetically alterable Ce^{3+}/Ce^{4+} redox couple.[7] The particle size of the inorganic particles plays a significant part in the enrichment of conductivity and electrolyte-electrode interfacial firmness at ambient temperature.[8] To carry out this task, numerous synthesis techniques such as co-precipitation, hydrothermal, sol-gel, microwave-assisted, and solvothermal methods are provided to synthesize cerium oxide nanofillers with various morphology and dimensions.[9,10]

Coprecipitation is broadly used to synthesize the consistent, large-pure material. This is a simple technique to scale up for mass production and cost-effectiveness. Ceria nanofillers were prepared with irregular morphology from $(NH_4)_2Ce(NO_3)_6$, ethylenediamine, and hydrazine using the hydrothermal method.[11] Ceria nanofillers were prepared using the coprecipitation method through changing temperature, atmosphere, and so forth.[12] Owing to restrict the agglomeration and particle growth is the key factor for controlling the size distribution, the first approach is based on lowering the critical concentration of the precursor source.[13] The precipitation agent base NaOH is a suitable catalyst because the dissociation of OH^- ions is maximum. The supplement of OH^- ions plays an important role to maintain the pH of the media, and also, it enhances the crystallinity and morphology of CeO_2 nanoparticles. Many pieces of literature are lacking to discuss the effect of concentration of NaOH on the preparation of CeO_2 nanoparticles. In this aspect, the present work focused the systematic studies on varying the concentration such as 0.5, 1, 1.5, and 2 M of (NaOH) capping agent named as CC1, CC2, CC3, and CC4, respectively, on synthesizing cubic structure CeO_2 nanoparticles. It has been employed by modified coprecipitation synthesis using an aqueous solvent. The as-prepared CeO_2 nanoparticles have been characterized using X-ray diffraction (XRD), FT-IR, laser Raman, scanning electron microscope (SEM), and photo luminescence (PL) analyses. The optimized materials are examined by transmission electron microscopy (TEM),

X-ray photoelectron spectroscopy (XPS), and energy dispersive X-ray spectroscopy (EDX) analyses. The optimized CeO_2 (0, 3, 6, 9, and 12) wt% is spread through the optimized P(S-MMA) (27 wt%)–$LiClO_4$ (8 wt%)–EC + PC (1;1 of 65 wt%) complex system by solution casting method. The as-prepared films are examined through the complex impedance analysis, and it also enhances the other electrochemical properties of the prepared electrolyte.

2 | MATERIALS AND METHODS

Cerium nitrate hexahydrate, sodium hydroxide, and poly(vinylpyrrolidone) have been utilized as raw constituents lacking extra refinement. The modified coprecipitation method was used to prepare CeO_2 nanofillers. To attain diverse morphology, 2.5 wt % of PVP[14] had been included to static content 0.2 M of $Ce(NO_3)_3.6H_2O$. The subsequent aqueous combination had been stimulated further for 10 min at 303 K, by adding 0.5-,1-, 1.5-, and 2-M NaOH added separately drip feed into the combination up to pH-12, which was reported in our previous literature.[15] The entire assortment had been stimulated for 1 h 30 min, additionally to acquire light yellow precipitate. The product had centrifuged (at 200 rpm) and washed with deionized water and acetone for numerous periods to get free of the remaining surfactant. Then the precipitate had been dehydrated in an oven at 383 K for 4 h, crushed the material for 30 m, and subsequently calcined in air at 600°C for 2 h to get Ceria material.[15]
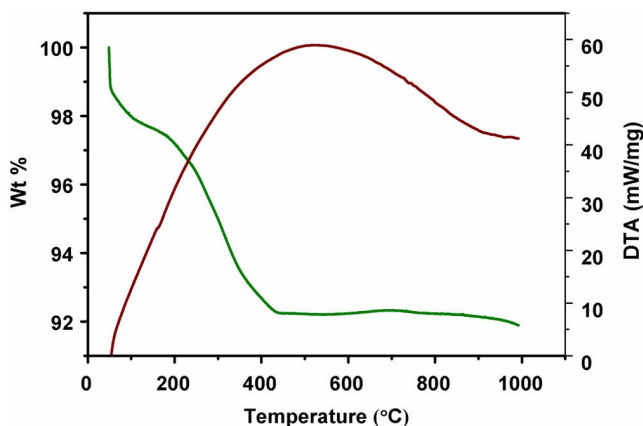
Poly(styrene-methyl metha acrolyte) P(S-MMA) (mol. wt. 100–150); Aldrich lithium perchlorate ($LiClO_4$); Aldrich. Ethylene carbonate EC (mol. wt. 88.06 g/mol); SRL. Propylene carbonate PC (mol. wt. 102.09 g/mol); SRL; India Tetra hydra furan (THF); Merck; Germany and as prepared 14-nm CeO_2 had been utilized as the preparatory constituents to make the composite gel polymer electrolyte. To synthesize P(S-MMA) (27 wt%)–$LiClO_4$ (8 wt%)–EC+PC (1;1 of 65 wt%)–(0, 3, 6, 9, and 12 wt%) CeO_2 polymer electrolyte, an appropriate amount of P(S-MMA), $LiClO_4$ was liquified in the THF and then the required amount of EC, PC, and CeO_2 were included in the assortment, which was magnetically stimulated at 303 K for 24 h, until the reliable solution was achieved. The subsequent mixture was cast on the Teflon plate and kept inside the vacuum oven for 12 h at 303 K, to allow the solvent to slowly evaporate. This procedure yielded free-standing film with an average thickness of 100–200 μm.

XRD analysis (Philips X'Pert PRO) with CuKα (45 kV, 50 mA) has examined the crystalline structure of the material at ambient temperature in the range of $20° \leq 2\theta \leq 80°$. The thermal history of the as-prepared precursor has been evaluated through TG/DTA (SHIMADZU DTG-60 AH). The thermogravimetric analysis (TGA) measurement was carried out in the temperature range from 30 to 1000°C at a heating rate

of 10°C/min under the air atmosphere. The molecular vibration of the material has been precisely measured by Fourier transform infrared (FT-IR) (Thermo Nicolet 380 spectrophotometer) in the range of 4000–400 cm^{-1}. The scanning electron microscope (SEM, Quanta FEG 200 with EDX) has been analyzed the surface morphology and size of the as-prepared samples. The high-resolution transmission electron microscopy (HR-TEM, FEI Techno F30 ST) technique has also been employed to calculate the particle size. The XPS PHI model 5802 has been used to analyze the electronic state of the elements. Photoluminescence spectroscopy (Bruin omega-10 spectrometer) has examined the presence of crystal defects in the prepared material. Keithley 3300 LCZ meter, performed the conductivity measurements in the frequency between 40 Hz and 100 kHz. The temperature of the film was varied between 25and 100°C. The as-prepared samples had been kept in the middle of the two stainless-steel electrodes, which accomplished as impeding terminal for the ions.
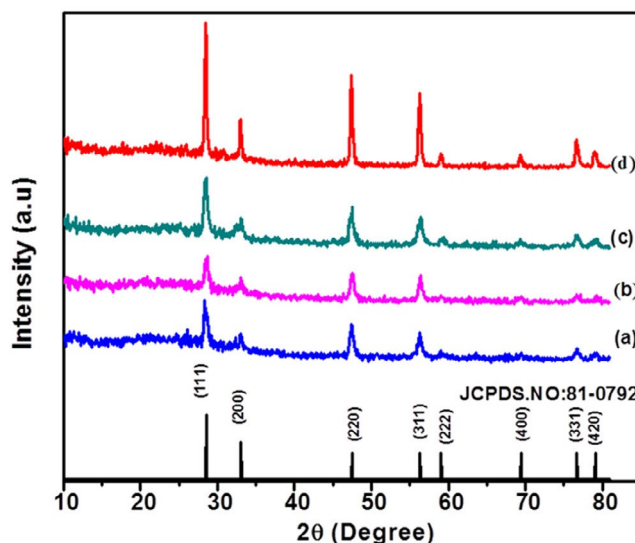
3 | RESULT AND DISCUSSION

The preparation of CeO$_2$ is being done by calcined the precursor at a temperature called formation temperature. This temperature has been determined through the thermal conversion process on the precursor using the aid of the TG/DTA study. TG/DTA curve of cerium nitrate precursor composed of surfactant and 0.5-M NaOH as precipitation agents is shown in Figure 1. There are three stages of weight loss observed in the TG curves: (i) 8% weight loss up to 100°C, (ii) 6% weight loss up to 400°C, and (iii) 5% weight loss up to 500°C. The initial mass reduction is ascribed to the physically absorbed humidity during the sample loading. The second stage of weight loss is due to the exclusion of nitrate compounds from the mixture and organic residue (i.e., PVP). The third weight loss is endorsed to the conversion process of cerium hydroxide into cerium oxide. A strong exothermic peak has also been observed at 590°C in the DTA curve, owing to the transformation from cerium hydroxide into cerium particles. The TG curve becomes nearly flat, which specifies that the precursor can be decomposed basically at 500°C, and extra heating only makes the assembly of the materials more crystalline. With this consideration, the calcination temperature has been preferred as 600°C for this sample. These values are comparable to the literature.[16,17]

The XRD pattern of CeO$_2$ by varying concentrations of precipitation agent (NaOH) such as 0.5, 1, 1.5, and 2 M with fixed content (0.2 M) of Ce(NO$_3$)$_3$.6H$_2$O are shown in Figure 2A–D along with the JCPDS standard. The characteristic peaks at $2\theta = 28.4°$, 32.8°, 47.3°, 56.3°, 58.9°, 69.5°, 76.5°, and 79.1° correspond to (111), (200), (220), (311), (222), (400), (311), and (420), respectively. All these peaks had been correlated (JCPDS # 81-0792) to the fcc phase with the space group Fm-3 m of CeO$_2$. None of the extra peaks related to impurities are observed. The diffraction pattern reveals that the crystallinity of the sample increases with an increase of precipitation agents up to 2 M. It may be due to the hydroxyl ions are in excess, pH value can nearly constant during the whole process. Consequently, for achieving uniform particles, 2 M of NaOH is employed to ensure the reaction at pH-12. Further, an increase in NaOH concentration and dissolution of nanocrystalline is possible. The lattice constant has been estimated $a = b = c = 5.425$ Å. The calculated unit cell parameters are somewhat larger than the literature values ($a = b = c = 5.412$ Å), which could be explained by lattice extension due to the small particle size.[18]

FIGURE 1 Thermogravimetic/differential thermal analysis (TG/DTA) curve of Ce(NO$_3$)$_3$. 6H$_2$O precursor prepared using NaOH as precipitation agent
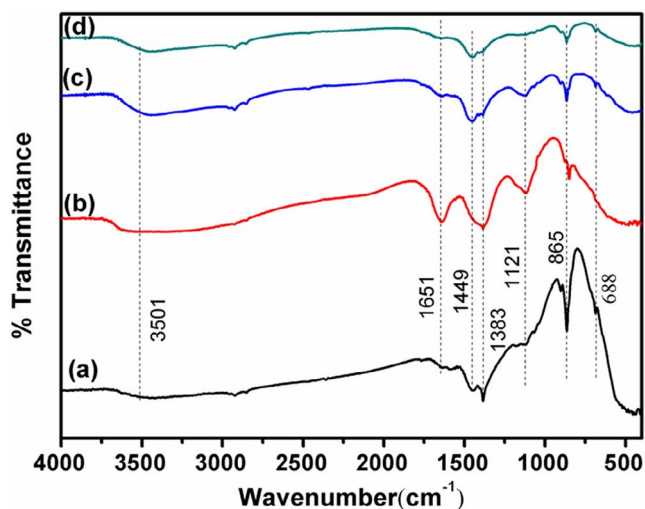

FIGURE 2 X-ray diffraction (XRD) patterns of ceria nanoparticles synthesized by varying NaOH as (A) 0.5 (CC1), (B) 1 (CC2), (C) 1.5 (CC3), and (D) 2 M (CC4) with 0.2-M Ce(NO$_3$)$_3$.6H$_2$O
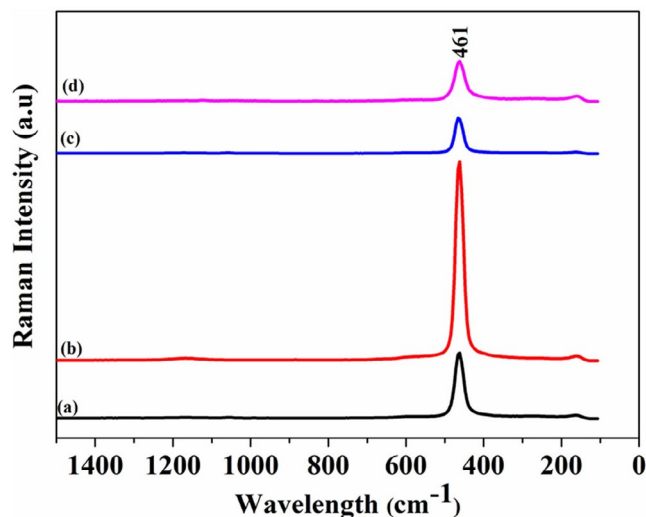
The crystalline domain size is determined as 13 nm by using Debye–Scherrer's formula.[19] Further, the dislocation density, strain, and cell volume have been calculated as 1.2983×10^{15}, 0.000893, and 159.69 $Å^3$, respectively. These values are comparable to the reported values.[20–22]

Figure 3A–D depicts the FT-IR spectra of the prepared CeO_2 fillers. The IR band at 3472 and 1393 cm^{-1} are attributed to the O–H elongating vibration and C–H deformation vibration mode, respectively. These peaks are shifted to (3443, 3375, 3438, and 3452 cm^{-1}) and (1383, 1387, 1382, and 1384 cm^{-1}) in the samples a, b, c, and d, respectively. The peak at 1450 cm^{-1} is ascribed to the C–H deformation mode. This peak is shifted to (1449, 1453, and 1458 cm^{-1}) for samples a, c, and d, respectively. The band around 2850 cm^{-1} is found in samples c and d due to the C–H bond of the CeO_2 nanoparticles with PVP characteristic peak.[23] The band due to Ce–O stretching vibration has been observed at 420 and 683 cm^{-1}. The band at 850 cm^{-1} reveals Ce–O metal-oxygen vibrations, which confirm the formation of CeO_2 particles. The bands are observed at (423, 480, 457, and 417 cm^{-1}), (686 and 697 cm^{-1}), (862, 848, 866, and 868 cm^{-1}) in the complexes. The assigned values were practically identical and agreed with literature data for CeO_2.[24,25]

The cubic structure of the CeO_2 nanoparticles has been further reinforced by the Raman spectra. Figure 4A–D illustrated the typical spectra of CeO_2. All the bands are observed at 461 cm^{-1}. This active Raman mode has attributed to the symmetrical breathing of the O atoms around each Ce^{4+} at 461 cm^{-1} that is the unit acceptable Raman mode with F_{2g} regularity in metal oxides with a fluoride structure. The vibrational mode is nearly independent of the cation mass.

FIGURE 4 Raman spectra of ceria nanoparticles synthesized by varying NaOH as (A) 0.5 (CC1), (B) 1 (CC2), (C) 1.5 (CC3), and (D) 2 M (CC4) with 0.2-M $Ce(NO_3)_3.6H_2O$
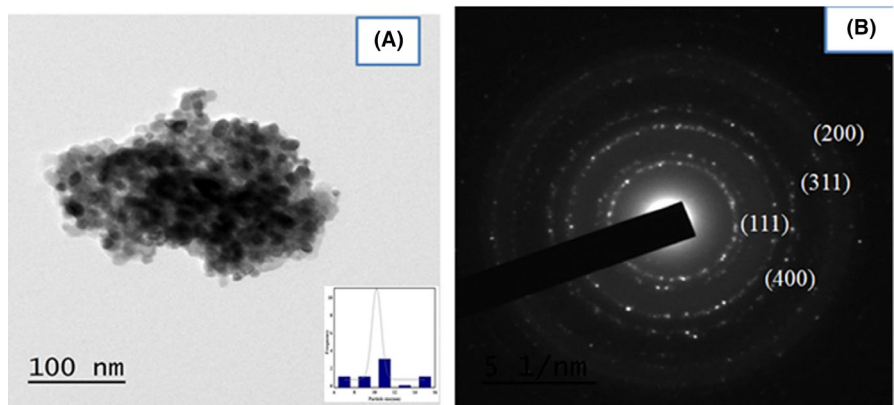

FIGURE 3 Fourier transform infrared (FT-IR) spectra of ceria nanoparticles synthesized by varying NaOH as (A) 0.5 (CC1), (B) 1 (CC2), (C) 1.5 (CC3), and (D) 2 M (CC4) with 0.2-M $Ce(NO_3)_3.6H_2O$

Figure 5A–E shows the SEM images and EDX profile of CeO_2 samples prepared using the modified coprecipitation method with the magnification of 5K. It is noticed from Figure 5 that the particle size increases upon the concentration of precipitation agent increased. The smaller particles are being the nutrients for the bigger particles as mentioned in the Oswald ripening[26] up to 1.0 M of NaOH. Beyond this content, the increase of NaOH causes a better supplement to the precipitation and makes the spherical particles and then the increment in concentration of NaOH enriches the particles in a spherical glory with the size of 180 nm. Hence, this material will be expected to have better electrochemical properties during the cycling upon use in the polymer matrices in the lithium battery manufacture. The creation of CeO_2 nanoparticles can be described by Oswald ripening. Nucleation and crystalline growth progressed under the precipitation route. At the initial stage $Ce(OH)_3$ was designed from $Ce(NO_3)_3$ in NaOH comprising environment. $Ce(OH)_3$ concentration reaches the supersaturated state in the calcination process and CeO_2 nuclei are formed. Small nanoparticles originate from the CeO_2 nuclei based on the Oswald ripening process in the MH system. The CeO_2 nanoparticles grow with the rises of NaOH content, consequently, CeO_2 nanoparticles with confined shape and size formed[27] and also it was alleged that the choosy fascination of 2.5 wt% PVP possesses steric effect and prevents aggregation, it absorbed on surfaces of crystallographic planes of CeO_2 changes the relative surface free energy of the facets and blocks sites essential to the incorporation of new growth units into the crystal lattice. Consequently, the crystal growth kinetics has been controlled and influences the size and product morphology.[28] Figure 5E shows the typical EDX spectrum of as-synthesized

FIGURE 5 Scanning electron microscope (SEM) images of ceria nanoparticles synthesized by varying NaOH as (A) 0.5 (CC1), (B) 1 (CC2), (C) 1.5 (CC3), (D) 2 M (CC4) with 0.2-M $Ce(NO_3)_3.6H_2O$, and (E) energy dispersive X-ray spectroscopy (EDX) spectrum of sample (CC4)
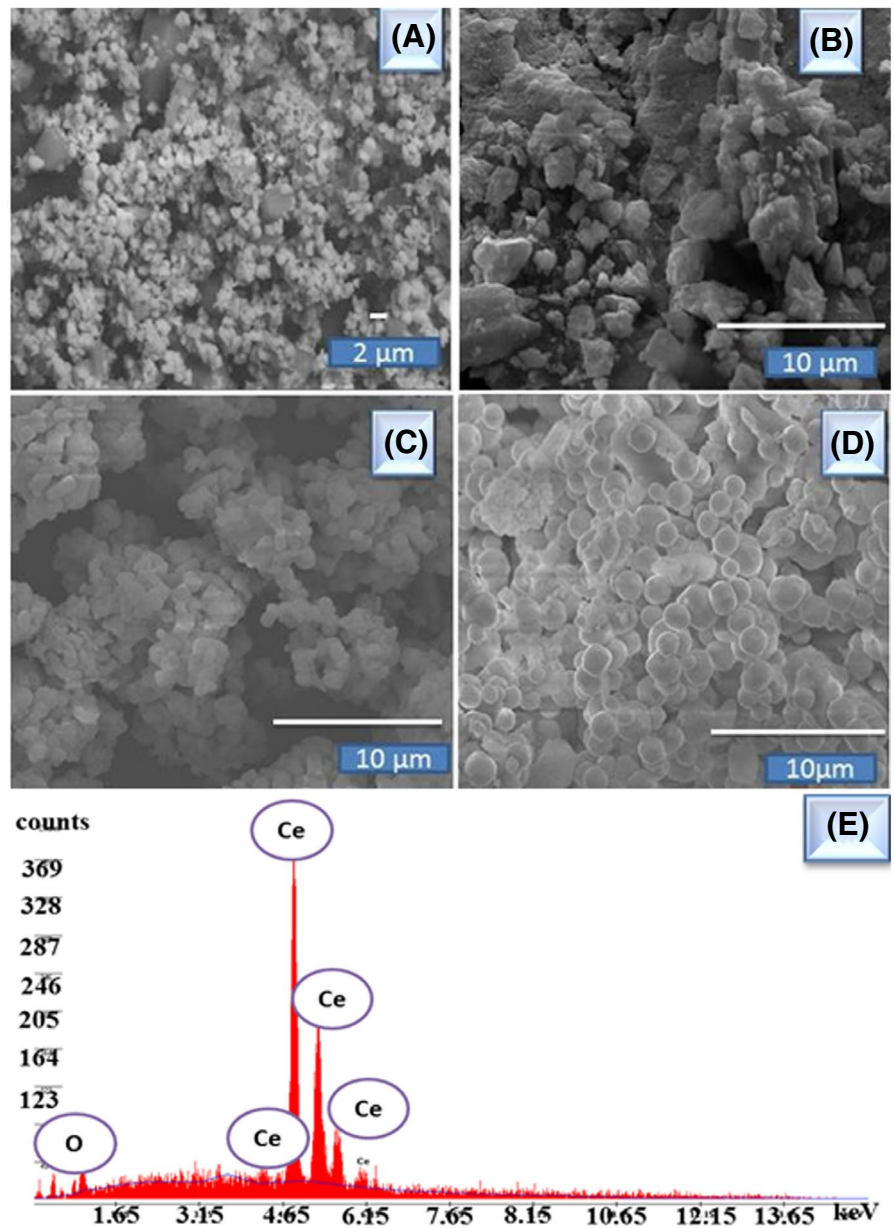
FIGURE 6 (A) Transverse electron microscopy (TEM) image with histogram and (B) selected area electron diffraction pattern of CC4
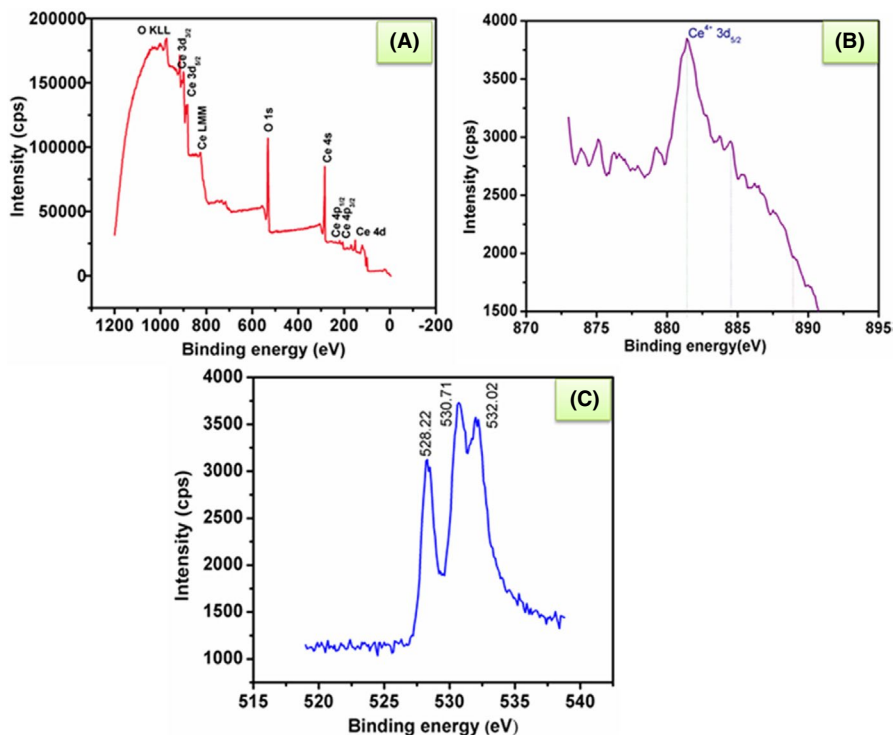
CeO_2 nanoparticles, which reveals that numerous distinct bands of Ce and O have atomic wt% of 95.51 (Ce L) and 4.49 (O K), respectively, and hence established that the as-prepared nanoparticles are made up of Ce and oxygen.

The HR-TEM image together with the selected area electron diffraction pattern of the as-prepared cerium oxide nanoparticles with 2 M of NaOH is depicted in Figure 6A,B. The TEM image of the augmented material has been depicted in Figure 6A. It shows the undeviating spreading of the particle laterally through its magnitude and outline. The measure IT software determines the particle size to confirm a consistent illustration of the definite size determination, and the projected particle size has been around 14 nm. The hologram of CeO_2 nanoparticles is shown in Figure 6A inset. The corresponding diffraction pattern shown in Figure 6B displays the existence of some pure spots laterally concerning diffusion circles; these rings revealed that the prepared sample has crystalline nature. The minimum distance between values is well associated with interplanar distances of XRD. It is clear that 2-M NaOH concentration has hydroxyl ions are in large; the pH value can nearly remain constant during the whole process.

To gain further information into the chemical composition of Ce and O in CeO_2 nanoparticles, the sample CC4 is examined using XPS analysis. Figure 7A–C shows the high-resolution satellite, Ce core, and O1s X-ray photoelectron spectra. The species Ce4d, Ce4s, O1s, Ce3d$_{5/2}$, and Ce3d$_{3/2}$ have been revealed in Figure 7A (wide range scanning XPS spectrum). The binding energy at 882.5 and 888.5 eV show the symmetric peaks of Ce^{4+} 3d$_{3/2}$ and Ce^{4+}3d$_{5/2}$, respectively. The spin-orbit split energy has been around 6 eV for the material. All the binding energy values that existed in the present study are in line with the earlier literature.[29–31] The oxygen binding energy O1s is superposed about 530.7 eV with additional two peaks on lower and higher sides; it is exposed in Figure 7C. The large binding energy has been documented to chemisorbed oxygen that is acknowledged to be the oxidation activity. The lesser binding energy is corresponding to the lattice oxygen in Ceria.[29] The C1s peak is detected in the range of 280–295 nm.

PL spectra attained with a Xenon laser of 290 nm as the excitation source of the CeO_2 nanoparticles are shown in Figure 8A–D at ambient temperature. The spectra of the whole materials have been nearly indistinguishable and primarily comprise of three emission bands: the solid band at 484 nm (2.56 eV), a feeble blue band at 419 nm (2.96 eV), and 369 nm (3.36 eV). All the obtained results are following the literature. The band appeared at 369 nm with the corresponding energy of 3.36 eV, which attributes band to band transition. It is higher than bulk CeO_2 (3.19 eV). The peaks at 484 and 419 nm reveal green and blue emission, respectively, which can be revealed the occurrence of oxygen defects. It may be due to the nonappearance of oxygen atom the crystal lattice; negative charge carriers will be inhibited to the vacancy sites and rise the local charge density. It is a favorable factor for our prepared filler.

The concentration of the conducting species and their mobility have been influenced the ionic conductivity of the polymer electrolyte. The ionic conductivity of the electrolyte was calculated by using the relation $\sigma = 1/R_b A$, where σ is the ionic conductivity, l the thickness of the sample, A the area
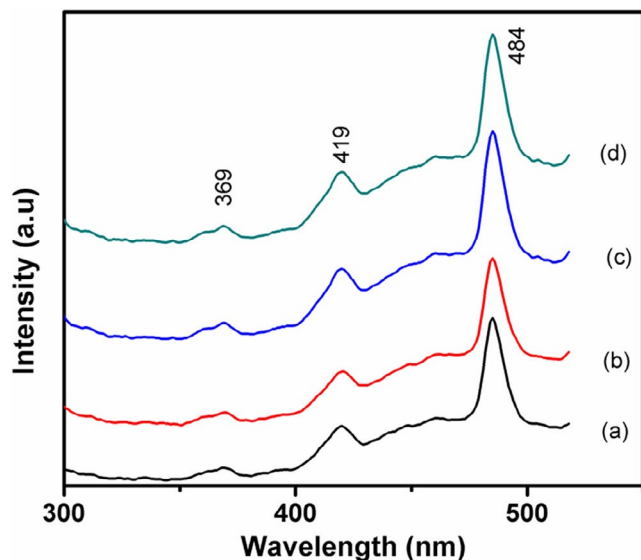
FIGURE 8 Photo luminescence spectra of ceria nanoparticles synthesized by varying NaOH as (A) 0.5 (CC1), (B) 1 (CC2), (C) 1.5 (CC3), and (D) 2 M (CC4) with 0.2-M $Ce(NO_3)_3.6H_2O$

FIGURE 9 Complex impedance plot of P(S-MMA) (27 wt%)–$LiClO_4$ (8 wt%)–EC + PC (65 wt%)–6 wt% CeO_2 polymer electrolyte system with varying temperature 303–353 K

of the cross section of the film, and R_b the bulk resistance, which is obtained from the intercept of the complex impedance plot. The plot for the P(S-MMA)-$LiClO_4$–EC + PC–CeO_2 (6 wt%) complex in the temperature range 303–353 K is shown in Figure 9. Theoretically, for symmetric cells consisting of stainless steel electrodes, the impedance spectrum appears as two portions; one is at the high-frequency semicircles corresponding to the bulk electrolytes impedance and the other at low frequencies straight line parallel to imaginary axis related to the interfacial impedance.

In the present study, the higher frequency semicircular portion such as the current carriers is the ions, and also, the total ionic conductivity is mainly the result of ion conduction.[32] The maximum ionic conductivity value was obtained for the sample containing 6 wt% of CeO_2 complex. This value is 8.13×10^{-4} S cm^{-1} at 303 K is higher than 2 orders of magnitude of the parent polymer electrolyte.[33] The maximum conductivity values for the film may be attributed to the following reasons: (i) the low molecular weight plasticizers such as EC and PC and also high dielectric constant of EC, which provides enough charge carriers and more mobile medium of the cations[34]; and (ii) the inclusion of nanofiller CeO_2 retards the recrystallization of polymer chains. Because the size of the filler is very small compared to the polymer host, the filler can penetrate the polymer matrix and promotion of interaction between filler, plasticizer, and polymer chain molecules; consequently, the cohesion force between the polymer chains is reduced and provides a more flexible chain segmental motion.[35,36] Hence, the ionic conductivity and mechanical stability of the polymer electrolyte are enhanced.
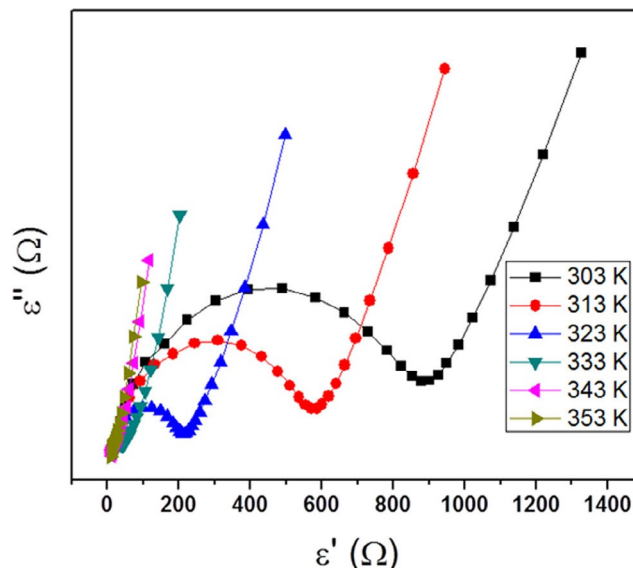
4 | CONCLUSION

The Ceria nanoparticles are successfully prepared via the modified coprecipitation method using 0.2 M cerium nitrate $Ce(NO_3)_3.6H_2O$ with various concentrations such as 0.5, 1, 1.5, and 2 M of NaOH as precipitation agent and 2.5 wt% of PVP molecule as starting material. The cubic structure with Fm-3m space group has been confirmed through (JCPDS: 81-0792) XRD analysis. Further, the presence of Ce and O species has been found through FT-IR, EDX, and XPS analyses. The morphology of CeO_2 nanoparticles was highly dependent on the concentration of sodium hydroxide. The increment in concentration of 2-M NaOH enriches the particles in a homogeneous spherical morphology with the size of 14 nm. Also, it has an energy gap of 3.38 eV, which is lesser than bulk. The optimized CeO_2 (0, 3, 6, 9, and 12) wt% is spread through the optimized P(S-MMA) (27 wt%)–$LiClO_4$ (8 wt%)–EC + PC (1;1 of 65 wt%) complex system by solution casting method. The maximum ionic conductivity value was obtained for the sample containing 6 wt% of CeO_2 complex. This value is 8.13×10^{-4} S cm^{-1} at 303 K. Hence, this material will be expected to have better electrochemical properties during the cycling upon use in the polymer electrolyte in the lithium battery assembly.

ORCID

Sivakumar Marimuthu https://orcid.org/0000-0002-7138-8220

REFERENCES

1. Beltrán-Gastélum M, Salazar-Gastélum MI, Flores-Hernández JR, Botte GG, Pérez-Sicairos S, Romero-Castañon T, et al. Pt-Au nanoparticles on graphene for oxygen reduction reaction: stability and performance on proton exchange membrane fuel cell. Energy. 2019;181:1225–34.
2. Hema M, Tamilselvi P. Lithium ion conducting PVA:PVdF polymer electrolytes doped with nano SiO_2 and TiO_2 filler. J Phy Chem Solids. 2016;96–97:42–8.
3. Yap YL, You AH, Teo LL. Preparation and characterization studies of PMMA–PEO-blend solid polymer electrolytes with SiO_2 filler and plasticizer for lithium ion battery. Ionics. 2019;25(7):3087–98.
4. Xie Z, Wu Z, An X, Yue X, Xiaokaiti P, Yoshida A, Abudula A, et al. A sandwich-type composite polymer electrolyte for all-solid-state lithium metal batteries with high areal capacity and cycling stability. J Membr Sci. 2020;596:117739.
5. Kitsou I, Arkas M, Tsetsekou A. Synthesis and characterization of ceria-coated silica nanospheres: their application in heterogeneous catalysis of organic pollutants. SN Appl Sci. 2019;1(12):1557.
6. Fu Q, Deng W, Saltsburg H, Flytzani-Stephanopoulos M. Activity and stability of low-content gold–cerium oxide catalysts for the water–gas shift reaction. Appl Catal B: Environ. 2005;56(1–2):57–8.
7. Sasmaz E, Wang C, Lance MJ, Lauterbach J. In situ spectroscopic investigation of a Pd local structure over Pd/CeO_2 and $Pd/MnO_x–CeO_2$ during CO oxidation. J Mater Chem A. 2017;5(25):12998–3008.
8. Yuan C, Li J, Han P, Lai Y, Zhang Z, Liu J. Enhanced electrochemical performance of poly(ethylene oxide) based composite polymer electrolyte by incorporation of nano-sized metal-organic framework. J Power Sources. 2013;240:653–8.
9. Zeng C, Tong K, Zhang M, Huang Q, Su Z, Yang C, et al. The effect of sol-gel process on the microstructure and particle size of ZrC–SiC composite powders. Ceram Int. 2020;46(4):5244–51.
10. Abu E-FA, Eltokhey AM, Abu-Sehley AA, El-Attar HM. Fabrication and analysis of the structural phase transition of ZrO_2 nanoparticles using modified facile sol–gel route. Phase Transit. 2019;92(1):36–51.
11. Panahi-Kalamuei M, Alizadeh S, Mousavi-Kamazani M, Salavati-Niasari M. Synthesis and characterization of CeO_2 nanoparticles via hydrothermal route. J Indus Eng Chem. 2015;21:1301–5.
12. Chen H-I, Chang H-Y. Synthesis of nanocrystalline cerium oxide particles by the precipitation method. Ceram Int. 2005;31(6):795–802.
13. Zhaohui WU, Yang S, Wu W. Shape control of inorganic nanoparticles from solution. Nanoscale. 2016;8(3):1237–59.
14. Lakhwani S, Rahaman MN. Adsorption of polyvinylpyrrolidone (PVP) and its effect on the consolidation of suspensions of nanocrystalline CeO_2 particles. J Mater Sci. 1999;34(16):3909–12.
15. Ramachandran M, Subadevi R, Sivakumar M. Role of pH on synthesis and characterization of cerium oxide (CeO_2) nano particles by modified co-precipitation method. Vacuum. 2019;161:220–4.
16. Maensiri S, Masingboon C, Laokul P, Jareonboon W, Promarak V, Anderson PL, et al. Egg white synthesis and photoluminescence of platelike clusters of CeO_2 nanoparticles. Cryst Growth Des. 2007;7(5):950–5.
17. Tok AIY, Boey FYC, Dong Z, Sun XL. Hydrothermal synthesis of CeO_2 nano-particles. J Mater Process Technol. 2007;190(1–3):217–22.
18. Zdravković J, Simović B, Golubović A, Poleti D, Veljković I, Šćepanović M, et al. Comparative study of CeO_2 nanopowders obtained by the hydrothermal method from various precursors. Ceram Int. 2015;41:1970–9.
19. Goharshadi EK, Samiee S, Nancarrow P. Fabrication of cerium oxide nanoparticles: Characterization and optical properties. J Colloid Interface Sci. 2011;356(2):473–80.
20. Naganuma T. Shape design of cerium oxide nanoparticles for enhancement of enzyme mimetic activity in therapeutic applications. Nano Res. 2017;10(1):199–217.
21. Wang ZL, Feng X. Polyhedral shapes of CeO_2 nanoparticles. J Phys Chem B. 2003;107(49):13563–6.
22. Balamurugan S, Parthiban P, Gopalakrishnan M, Senthilkumar K, Palanisami N. Optical, photocatalytic and (micro)-structural studies of ball milled CeO_2 nanomaterials. Adv Sci Eng Medi. 2014;6(9):991–1000.
23. Zhou F, Zhao X, Xu H, Yuan C. CeO_2 spherical crystallites: synthesis, formation mechanism, size control, and electrochemical property study. J Phys Chem C. 2007;111(4):1651–7.
24. Patil S, Sandberg A, Heckert E, Self W, Seal S. Protein adsorption and cellular uptake of cerium oxide nanoparticles as a function of zeta potential. Biomaterials. 2007;28(31):4600–7.
25. Tong S, Deng H, Wang L, Huang T, Liu S, Wang J. Multi-functional nanohybrid of ultrathin molybdenum disulfide nanosheets decorated with cerium oxide nanoparticles for preferential uptake of lead (II) ions. Che Eng J. 2018;335:22–31.
26. Wang G, Mu Q, Chen T, Wang Y. Synthesis, characterization and photoluminescence of CeO_2 nanoparticles by a facile method at room temperature. J Alloys Compds. 2010;493(1–2):202–7.
27. Phuruangrat A, Thongtem T, Thongtem S. Effect of NaOH on morphologies and photocatalytic activities of CeO_2 synthesized by microwave-assisted hydrothermal method. Mater Lett. 2017;193:161–4.
28. Phoka S, Laokul P, Swatsitang E, Promarak V, Seraphin S, Maensiri S. Synthesis, structural and optical properties of CeO_2 nanoparticles synthesized by a simple polyvinyl pyrrolidone (PVP) solution route. Mater Chem Phys. 2007;115(1):423–8.
29. Wang N, Li S, Zong Y, Yao Q. Sintering inhibition of flame-made Pd/CeO_2 nanocatalyst for low-temperature methane combustion. J Aerosol Sci. 2017;105:64–72.
30. Ferreira NS, Angélica RS, Marques VB, de Lima CCO, Silva MS. Cassava-starch-assisted sol–gel synthesis of CeO_2 nanoparticles. Mater Lett. 2016;165:139–42.
31. Dutta P, Pal S, Seehra MS, Shi Y, Eyring EM, Ernst RD. Concentration of Ce^{3+} and oxygen vacancies in cerium oxide nanoparticles. Chem Mater. 2006;18(21):5144–6.

32. Rui M, Ma C, Tang X, Yang J, Jiang F, Pan Y, et al. Phytotoxicity of silver nanoparticles to Peanut (*Arachis hypogaea* L.): physiological responses and food safety. ACS Sustainable Chem Eng. 2017;5:6557–67.

33. Rajendran S, Sivakumar M, Subadevi R. Investigations on the effect of various plasticizers in PVA–PMMA solid polymer blend electrolytes. Mater Lett. 2004;58(5):641–9.

34. Selvasekarapandian S, Baskaran R, Hema M. Complex AC impedance, transference number and vibrational spectroscopy studies of proton conducting PVAc–NH4SCN polymer electrolytes. Physica B: Condens Matter. 2005;357(3–4):412–9.

35. Wang Z, Yu R. Hollow micro/nanostructured ceria-based materials: Synthetic strategies and versatile applications. Adv Material. 2019;31(38):1800592.

36. Gohel K, Kanchan DK. Effect of PC:DEC plasticizers on structural and electrical properties of PVDF–HFP:PMMA based gel polymer electrolyte system. J Mater Sci: Mater Electron. 2019;30:12260–8.